ACS OMEGA

http://pubs.acs.org/journal/acsodf

Article

Long-Term Evolution of Vacancies in Large-Area Graphene

Shihao Su, Yong Liu, Man Li, Huaqing Huang, and Jianming Xue*

Cite This: *ACS Omega* 2022, 7, 36379−36386

Read Online

ACCESS | Metrics & More | Article Recommendations | Supporting Information

ABSTRACT: Devices based on two-dimensional (2D) materials such as graphene and molybdenum disulfide have shown extraordinary potential in physics, nanotechnology, and electronics. The performances of these applications are heavily affected by defects in utilized materials. Although great efforts have been spent in studying the formation and property of various defects in 2D materials, the long-term evolution of vacancies is still unclear. Here, using a designed program based on the kinetic Monte Carlo method, we systematically investigate the vacancy evolution in monolayer graphene on a long-time and large spatial scale, focusing on the variation of the distribution of different vacancy types. In most cases, the vacancy distribution remains nearly unchanged during the whole evolution, and most of the evolution events are vacancy migrations with a few being coalescences, while it is extremely difficult for multiple vacancies to dissolve. The probabilities of different categories of vacancy evolutions are determined by their reaction rates, which, in turn, depend on corresponding energy barriers. We further study the influences of different factors such as the energy barrier for vacancy migration, coalescence, and dissociation on the evolution, and the coalescence energy barrier is found to be dominant. These findings indicate that vacancies (also subnanopores) in graphene are thermodynamically stable for a long period of time, conducive to subsequent characterizations or applications. Besides, this work provides hints to tune the ultimate vacancy distribution by changing related factors and suggests ways to study the evolution of other defects in various 2D materials.

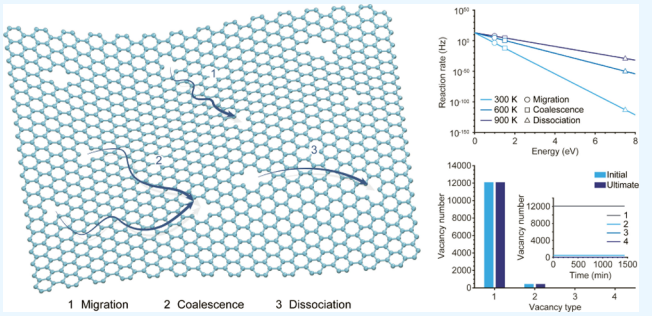

1. INTRODUCTION

Two-dimensional (2D) materials such as graphene have attracted broad interest in electronic components,[1,2] water desalination,[3,4] matter separation,[5,6] and nanofluidic devices.[7,8] The application performances are determined by the material structures, where the existence of defects has extremely important influences on their physical and chemical properties.[9,10] In electronics and optics, doped and attached atoms to transition-metal dichalcogenides affect the magnetic moments, band gap, and excitons of the materials.[11,12] Monovacancies in graphene are crucial to achieve exponentially selective molecular sieving (e.g., helium and hydrogen against xenon and methane).[13] Stone−Wales defects lead to the ultrafast and selective transport of proton of monolayer graphene.[14] In water desalination and ion separation, high-density subnanometer pores (which are essentially vacancies) with narrow size distribution make 2D materials ideal for next-generation separation membranes with high water permeance, excellent salt rejection, and considerable ion selectivity.[15,16] Nanopores with a stable structure and controllable size are keys to fabricate sensitive 2D molecule sensors.[17,18] Therefore, studies on the formation, evolution, and property of various defects in 2D materials are especially significant for understanding their atomistic mechanisms and improving the performances of related devices.

Previous research studies mainly focus on the formation and property of defects in 2D materials, while their evolution has received less attention, especially on a long time and large spatial scale.[19−22] Recently, Vinchon et al.[23] have investigated the evolution of adatoms and grain boundaries and experimentally reported the preferential self-healing at grain boundaries due to the migration of adatoms and the structural recovery in plasma-treated graphene using hyperspectral Raman imaging, which provides sensitive mapping on a large area (130 × 130 μm^2) and a long timescale (hundreds of seconds). However, the long-term evolution of vacancies in large-area 2D materials remains elusive, limited by experimental techniques such as the electron beam-induced ejection of atoms at the edge of graphene pores during the imaging using a transmission electron microscope.[24,25] Theoretical methods such as classical molecular dynamics (MD) simulations and density functional theory (DFT) calculations have been utilized to study vacancy evolutions in 2D materials,[19,21] but they can hardly simulate the evolutions on

Received: June 30, 2022
Accepted: September 20, 2022
Published: October 4, 2022

https://doi.org/10.1021/acsomega.2c04121
ACS Omega 2022, 7, 36379−36386

a long timescale (>1 ms). In MD simulations, extremely short time steps (∼1 fs) are normally employed to accurately simulate the atom thermal vibrations, which consequently limits the simulation time to less than 1 μs.[26] DFT calculations also have the above "timescale" limitation, and they can only study systems with atoms less than 1000.[27] Hence, DFT is generally used to calculate the energy barriers for vacancy evolutions such as migration and coalescence.[28]

The kinetic Monte Carlo (KMC) method is powerful to simulate systems on a long timescale which can be days or even years because only effective events (the transition from a metastable state to another one) are taken into account, while others (thermal oscillation movements) are neglected.[26] This method has been successfully utilized to study the long-term evolution of various systems, such as the dynamics of impurity atoms and point defects in bulk materials,[29,30] the growth and etching of 2D materials,[31−33] and the transport phenomenon in silicon heterojunction solar cells.[34] However, KMC simulations on the evolution of vacancies in 2D materials are rare and controversial.[35,36] Trevethan et al.[35] reported that the migration and coalescence of monovacancies can only generate vacancy lines in monolayer graphene, while thermodynamically stable multiple vacancy structures such as holes are kinetically inaccessible. Nevertheless, Parisi et al.[36] found that large round and parallelogram nanopores can form as a result of monovacancy attachments to preformed pores, that is, the coalescence of vacancies. Whether monovacancies can coalesce into multiple vacancies or not is crucial for understanding the stability of the distributions of vacancies in 2D materials.

Here, we systematically investigate the long-term evolution of vacancies in large-area monolayer graphene using a designed KMC program. Three categories of vacancy evolutions (migration, coalescence, and dissociation) are considered, whose reaction rates are characterized by corresponding energy barriers. In most cases, the ultimate vacancy distribution (number of different vacancy types) after the vacancy evolution is nearly the same as the one at the beginning, showing the stability of vacancy distribution in graphene. The influences of different factors such as initial vacancy proportion, energy barriers for vacancy migration, coalescence, dissociation, and temperature on vacancy evolution are studied, and the energy barrier for vacancy coalescence is found to play a leading role in the whole evolution.

2. RESULTS AND DISCUSSION

2.1. Vacancy Evolutions Concerned in the KMC Simulations. The evolutions of vacancies in graphene include reconstruction, migration, coalescence, and dissociation.[19,21] The reconstruction only affects the local structure of a vacancy, for example, the transition between V_2(5-8-5) and V_2(555-777), and it hardly influences the vacancy type (identified by the number of missed atoms in this work), not to mention the distribution of vacancies (the numbers of different vacancy types). This work aims at the long-term evolution of vacancies, in which the variation of vacancy distribution is much more crucial than the vacancy structures. Therefore, the vacancy reconstruction is neglected in our KMC simulations, and the migration, coalescence, and dissociation are concerned, which are schematically illustrated in Figure 1. In addition, vacancy structures are not taken into consideration, which indicates that the vacancy (nanopore) isomers[37] are also neglected here.

To simulate the evolution of vacancies in graphene, a designed program based on the KMC method is employed.

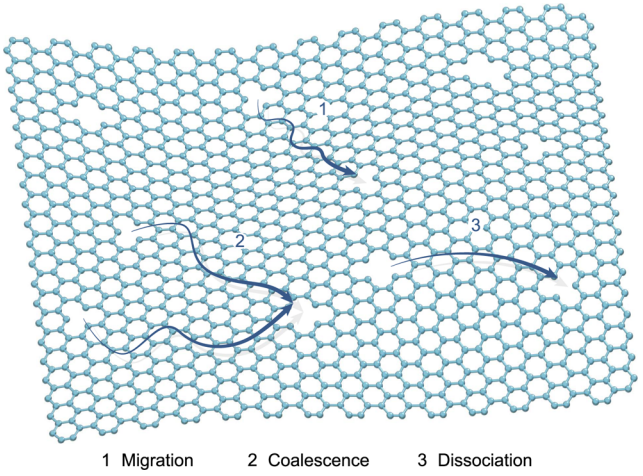

Figure 1. Schematic illustration of three categories of vacancy evolutions in graphene. 1, Migration of monovacancy. 2, Coalescence of one monovacancy and another vacancy (which can be single or multiple). 3, Dissociation of bivacancy.

Figure 2 shows the algorithm flowchart of the program. First, the system is initialized to create the initial vacancies in the graphene, where a portion of carbon atoms are randomly and uniformly removed, characterized by the initial vacancy proportion α (e.g., α = 1% indicates that 1% carbon atoms are removed from the pristine graphene). Meanwhile, the event table is established as shown in Table 1, which consists of all the possible evolution events (migration, coalescence, and dissociation) of the vacancies. For vacancy j, its current coordinate is (x_j, y_j), and it can, for example, migrate to a new coordinate $(x_{j,i}, y_{j,i})$. This migration evolution event i has the energy barrier E_i and the reaction rate ν_i. In addition, the vacancy j can also, if possible, migrate to another new coordinate $(x_{j,i+1}, y_{j,i+1})$, representing the migration evolution event i + 1. The reaction rate of the event i can be estimated from the Arrhenius formula[38] as shown in eq 1

$$\nu_i = A \cdot \exp\left(-\frac{E_i}{k_B T}\right) \quad (1)$$

where A is the attempt frequency close to the thermal oscillation frequency of target atoms (which is about 10^{13} Hz for graphene[19,21,35,36]), k_B is the Boltzmann constant, and T is the temperature. After initialization, the KMC program enters the main loop procedure until reaching the convergence condition that the system is stable and the vacancy distribution remains unchanged for a long time (1 day) or the maximum step/loop of 1×10^7 limited by the computing resources (which is rarely reached). At the beginning of every loop, an event i is randomly selected from the event table (Table 1) with its reaction rate as the weight, that is, the probability of the event p_i is calculated by $p_i = \nu_i / \sum_{k=1}^{N} \nu_k$, where N is the total number of all the events. This event is then realized, and the coordinate of the vacancy is changed to the new one. The elapsed time for the event τ (which corresponds to the duration of the event under experimental conditions) can be estimated by $\tau = -\ln\xi / \sum_{k=1}^{N} \nu_k$, where ξ is a random number evenly distributed in the range of (0, 1) generated in the current loop.[21,30,39,40] At the end of the loop, the event table is updated because the vacancy distribution in the graphene has changed. Additional details about the program and simulations can be found in Methods.

https://doi.org/10.1021/acsomega.2c04121
ACS Omega 2022, 7, 36379−36386

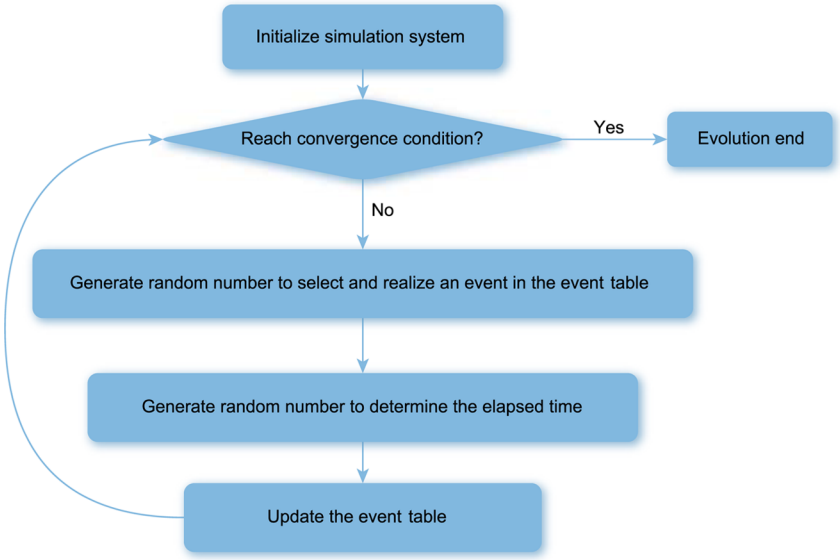

Figure 2. Flowchart of the algorithm of the KMC simulation program. First, the simulation system with certain vacancies in the graphene is initialized, and meanwhile, the event table is created based on the vacancy distribution. The program then enters the main loop until reaching the convergence condition and finishing the evolution. At the beginning of each loop, an event in the event table is randomly selected according to its reaction rate and realized. Then, the elapsed time for this event is calculated. After the event is realized, the vacancy distribution of the system has changed, and thus, the event table is updated before the next loop.

Table 1. Event Table

event	vacancy	current coordinate	new coordinate	energy barrier	reaction rate
i	j	(x_j, y_j)	$(x_{j,i}, y_{j,i})$	E_i	ν_i
$i+1$	j	(x_j, y_j)	$(x_{j,i+1}, y_{j,i+1})$	E_{i+1}	ν_{i+1}
$i+2$	$j+1$	(x_{j+1}, y_{j+1})	$(x_{j+1,i+2}, y_{j+1,i+2})$	E_{i+2}	ν_{i+2}

The simulated graphene is a rhombus with a length of 123.022 nm and a height of 106.54 nm, consisting of 500 × 500 rhombic primitive cells with 500,000 carbon atoms in total, which is comparable to the grain size of monolayer graphene in experiments (in the order of μm) and much larger than the graphene size in previous MD and DFT simulations.[21] It is worth noting that the size of the graphene is properly selected to ensure that sufficient random events of vacancy evolutions can be sampled and also to optimize computing resources (see details in Methods).

2.2. Stability of Vacancy Distribution. In the KMC simulations, the reaction rates of different categories of vacancy evolutions are determined by corresponding energy barriers according to eq 1. The energy barriers for vacancy migration (E_m), coalescence (E_c), and dissociation (E_d) are schematically diagramed in Figure 3a. In monolayer graphene, previous DFT calculations have given that $E_m \approx 1.0$ eV, $E_c \approx 1.5$ eV, and $E_d \approx 7.5$ eV.[21] Figure 3b shows the reaction rate of each category of vacancy evolution under experimental conditions at different temperatures estimated from eq 1. The reaction rate exponentially depends on the energy barrier, and thus, a slight difference between the energy barriers can lead to a significant difference in the reaction rates. For example, at room temperature (T = 300 K), the reaction rate of vacancy migration is about 2.5 × 10^8 times faster than that of the coalescence, despite the small difference between E_c and E_m typically being 0.5 eV. As for the vacancy dissociation, $E_d \gg E_c$ (E_m), and thus, its reaction rate is extremely much slower than those of the others, which suggests that the dissociation of vacancies hardly happened, even at a high temperature (900 K) as shown in Figure 3b.

We first study the evolution of vacancies for a typical system with α = 2.6%, E_m = 1.0 eV, E_c = 1.5 eV, E_d = 7.5 eV, and T = 300 K. α = 2.6% represents an extremely high initial vacancy density of ∼1 × 10^{14} cm^{-2}, which has hardly been found in experiments,[22] and this value is utilized here in order to ensure the occurrences of sufficient random events of vacancy evolutions. Figure 3c shows the initial and ultimate vacancy distribution for the evolution of vacancies in graphene. In the initial distribution, most of the vacancies are monovacancies, and a small number of multivacancies exist because some of the carbon atoms in the pristine graphene were randomly removed at the beginning, which could generate multiple vacancies if adjacent atoms are removed together. After the long-term evolution of vacancies, the ultimate vacancy distribution is found to be the same as the initial one. Furthermore, the numbers of different types of vacancies do not change during the whole vacancy evolution as shown in the inset in Figure 3c, which indicates that no coalescence and dissociation of vacancies happened in the evolution except for the vacancy migration (see the proportions of three categories of vacancy evolutions in Figure 3d). For this system, it is not difficult for monovacancies to migrate due to its reaction rate of about 1.6 × 10^{-4} Hz, but the vacancy coalescence and dissociation are inaccessible for their much slower reaction rates as shown in Figure 3b). The migration of vacancies only influences the vacancy locations, and thus, the vacancy distribution remains unchanged. The results indicate that the vacancy distribution is thermodynamically stable during the long-term vacancy evolution.

Then, the influences of several factors (α, E_m, E_c, and T) on the evolution of vacancies in graphene are systematically investigated as shown in Figure 4. It is worth noting that to optimize computing resources, the dissociation of multiple vacancies is neglected in these simulations because it hardly happens due to its extremely slow reaction rate (see Figure

https://doi.org/10.1021/acsomega.2c04121
ACS Omega 2022, 7, 36379−36386

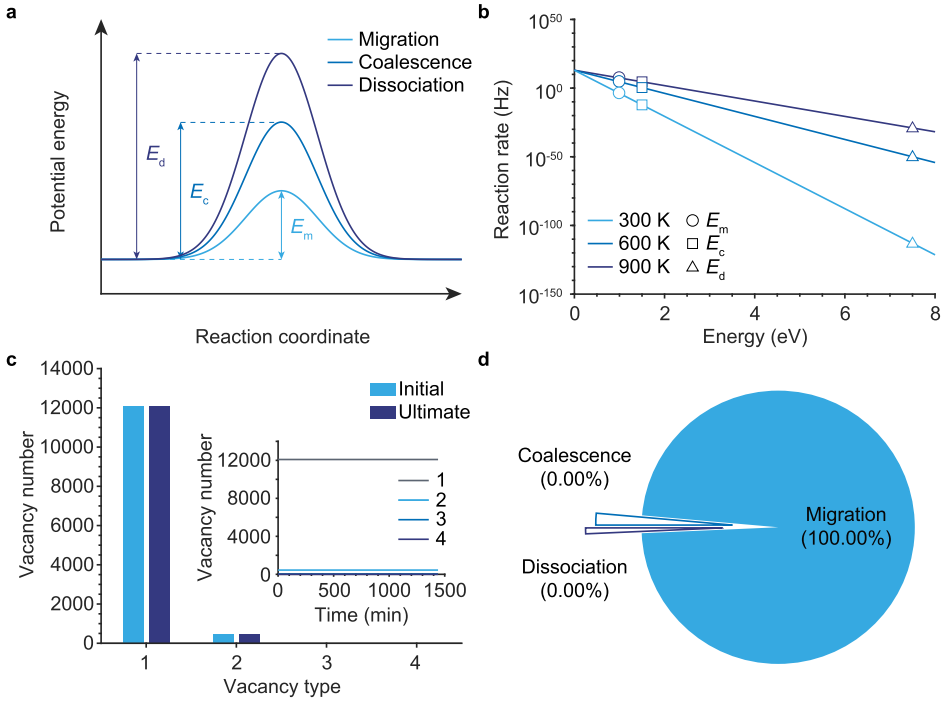

Figure 3. Evolution of vacancies in graphene. (a) Energy barrier profiles for three categories of vacancy evolutions (migration E_m, coalescence E_c, and dissociation E_d). (b) Reaction rates (under experimental conditions) of vacancy evolutions with different energy barriers estimated from eq 1 at different temperatures. The typical reaction rates of vacancy migration, coalescence, and dissociation are indicated by corresponding patches. (c) Distributions of vacancies before and after the long-term evolution of vacancies in graphene. The results are for the system with α = 2.6%, E_m = 1.0 eV, E_c = 1.5 eV, E_d = 7.5 eV, and T = 300 K. The inset shows the numbers of different vacancy types as the function of time (under experimental conditions) during the whole evolution. (d) Proportions of three categories of vacancy evolutions in (c).

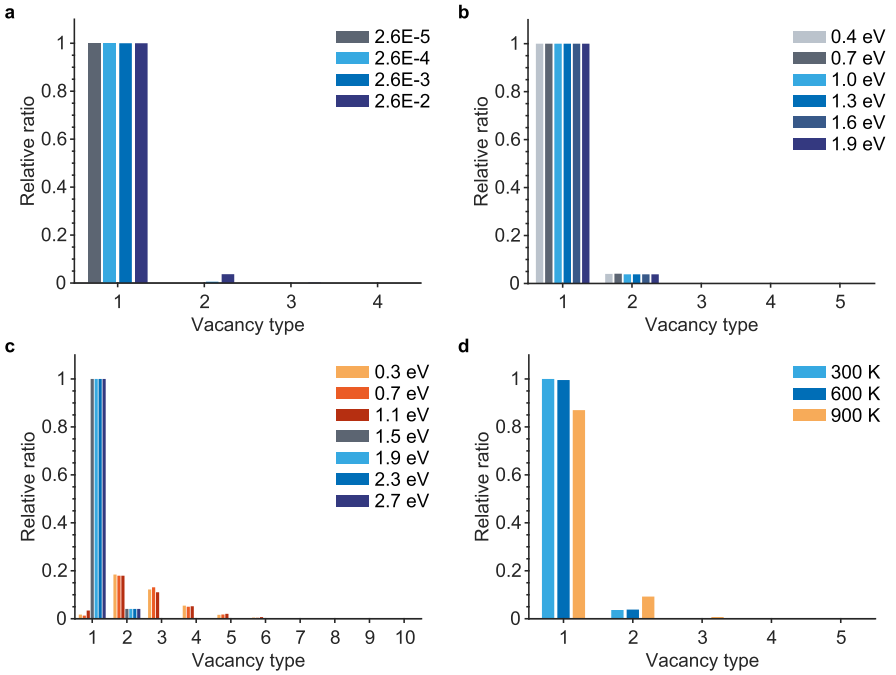

Figure 4. Influences of several factors on the evolution results of vacancies in graphene. The results are for the systems with different initial vacancy proportions α (a), energy barrier for vacancy migration E_m (b), energy barrier for vacancy coalescence E_c (c), and temperature T (d), where the controlled factors are α = 2.6%, E_m = 1.0 eV, E_c = 1.5 eV, and T = 300 K. The dissociation of multiple vacancies is neglected because it hardly happens as discussed in the article. Relative distributions of vacancy type (normalized by the number of initial monovacancies) after the long-term evolution of vacancies in graphene are shown here, and those before the evolution are omitted for clearness because they are nearly the same as that in Figure 3c.

3b). Figure 4a shows the ultimate relative vacancy distribution for different initial vacancy proportions α. Previous review[22] reported the maximum vacancy density in experiments to be the order of 10^{13} cm^{-2}, so a larger value of $\sim 1 \times 10^{14}$ cm^{-2} was

https://doi.org/10.1021/acsomega.2c04121
ACS Omega 2022, 7, 36379−36386

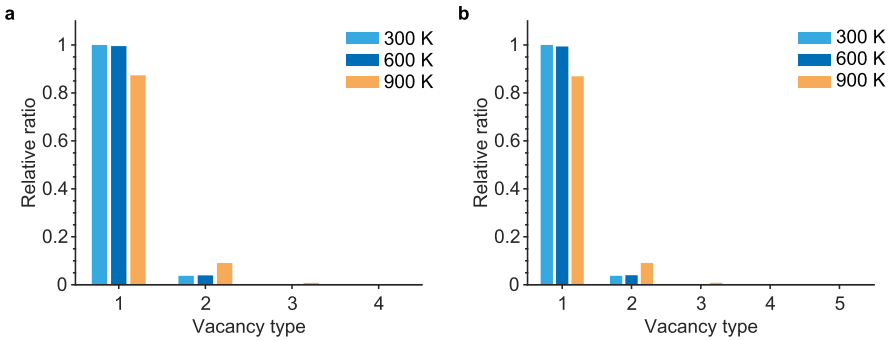

Figure 5. Influences of the energy barrier for vacancy dissociation on the evolution results of vacancies in graphene. The results are for the systems with E_d = 7 eV (a) and 6 eV (b), α = 2.6%, E_m = 1.0 eV, E_c = 1.5 eV, and different T. Relative distributions of vacancy type (normalized by the number of initial monovacancies) after the long-term evolution of vacancies in graphene are shown here, and those before the evolution are omitted for clearness because they are nearly the same as that in Figure 3c.

studied here (corresponding to α = 2.6%). Limited by the system size, the smallest vacancy density of $\sim 1 \times 10^9$ cm^{-2} was investigated (corresponding to $\alpha = 2.6 \times 10^{-5}$). Although a larger α indicates more initial vacancies and evolution events, the reaction rates of different categories of vacancy evolutions remain unchanged for various α (eq 1). Therefore, α has negligible influence on the ultimate vacancy distribution, which is similar to the influence of the graphene size with a high E_m (see Figure S1a).

Figure 4b shows the influence of the energy barrier for vacancy migration E_m on the ultimate vacancy distribution. E_m is not certain for monolayer graphene, and previous DFT calculations have reported the value to be 0.91−1.40 eV.[21] Therefore, we studied different E_m with a much wider range of 0.4−1.9 eV. According to eq 1, the smaller E_m is, the much faster the migration reaction rate becomes, which leads to more migration events in the whole vacancy evolution. In this case, only the probability of two vacancies meeting is increased, but whether they coalesce together or not primarily relies on the energy barrier for vacancy coalescence E_c. As a result, E_m shows a negligible influence on the ultimate vacancy distribution.

The energy barrier for vacancy coalescence E_c is found to be dominant for the ultimate vacancy distribution as shown in Figure 4c. We studied E_c in the range of 0.3−2.7 eV, which is also much wider than the reported value of 0.82−2.17 eV.[21] For a high E_c (1.5, 1.9, 2.3, and 2.7 eV), it is difficult for two vacancies to overcome this energy barrier and coalesce together. In such cases, the ultimate vacancy distribution is nearly the same as that at the beginning. Nevertheless, for a low E_c (0.3, 0.7, and 1.1 eV), the coalescence of two vacancies is likely to happen when they migrate as neighbors. Thus, many monovacancies coalesce with the others into bivacancies, which hardly migrate or dissolve, and a few multiple vacancies can also be generated as a result of the coalescence of monovacancies and other multivacancies. After the long-term vacancy evolution, the vacancy distribution is similar to a logarithmic one, where most of the vacancies are bivacancies and the larger vacancies are, the smaller their number becomes. Occasionally, we found multiple vacancies with 10 atoms missed, which is also termed a subnanopore. It is worth noting that the ultimate vacancy distributions for different low E_c are similar, which suggests the existence of a threshold value. For systems with E_c larger than it, the coalescence of vacancies hardly influences the distribution, while for systems with a smaller E_c, the vacancy coalescence plays a leading role in the long-term vacancy evolution, and the ultimate vacancy distribution is nearly the same. Such a threshold value of E_c and related mechanisms are beyond the scope of this work, and future research may focus on them.

In addition to the energy barriers for vacancy evolutions, temperature also affects the reaction rates as shown in eq 1 as well as Figures 3b, and 4d shows the ultimate vacancy distribution for systems at different temperatures. The reaction rates of both migration and coalescence increase with the increase in temperature, and therefore, more monovacancies migrate and coalesce together at a higher temperature, making the ultimate distribution different from that at the beginning. However, the influence of temperature on the vacancy distribution is slight, and most vacancies are still monovacancies when the whole evolution is finished. The results indicate that the vacancy distribution remains stable after the long-term vacancy evolution even at a high temperature. It is worth noting that our work focuses on the evolution of vacancies in monolayer graphene at different constant temperatures, and it is different from the heating or annealing processes in experiments, where complicated phenomena could appear, such as self-healing or reconstruction of defects.[41,42] Besides, the KMC simulations do not consider some factors in experiments (e.g., adsorptions on the graphene surface, gases in ambient conditions, thermal vibration of graphene carbon atoms), which could cause various effects on graphene defects at high temperatures. Although such investigations are valuable, they are beyond the scope of this work and could be studied in the future.

To further study the influence of the energy barrier for vacancy dissociation E_d on the evolution of vacancies, we simulated systems with lower E_d, and the results are shown in Figure 5. High temperature leads to fast reaction rates, so the results at different temperatures are presented there. The large difference (~6 eV) between E_d and E_m (or E_c) makes the reaction rate of dissociation extremely slower than that of migration or coalescence (tens of order as shown in Figure 3b). Therefore, it is very difficult for multiple vacancies to dissolve even at a high temperature and with a small E_d, and such events have hardly been found in our simulations. Indeed, the coalescence of vacancies is negligible during the long-term evolution of vacancies in monolayer graphene.

The above simulation results show the stability of vacancy distributions after the long-term vacancy evolution in monolayer graphene, which is also confirmed by our previous theoretical and experimental works on subnanopores fabricated

https://doi.org/10.1021/acsomega.2c04121
ACS Omega 2022, 7, 36379−36386

using the irradiation of energetic ions in monolayer graphene.[43,44] In the classical MD simulations, the irradiation of ions can directly generate subnanopores due to the cascade collisions, and most of the pores, which are essentially vacancies, are with several atoms removed.[43] Such theoretical predictions agreed with the pores observed in experiments using a scanning transmission electron microscope, where most subnanopores with several atoms missed were found.[44] Besides, the averaged pore diameter predicted in the MD simulations is 5 Å for Au ions with an energy of 500 keV, which is also consistent with our experimental result.[43,44] It is worth noting that in the MD simulations, vacancies (pores) fabricated under the ion irradiation have not undergone further thermodynamical evolution (migration, coalescence, and dissociation), which are similar to the initial vacancies in this work. The experimentally observed subnanopores were actually the results after the vacancy evolution because there is a long period of time (at least several hours) between the fabrication and observation of the pores, which is enough for the finishing of the evolution. Therefore, the similarity between the ultimate vacancy distribution in experiments and the initial one in MD simulations confirms the stable vacancy distribution during the long-term evolution as demonstrated in this work.

In conclusion, we systematically study the long-term evolution of vacancies in large-area monolayer graphene using the KMC method. The ultimate vacancy distribution after the evolution is nearly the same as the initial one in most cases, which indicates the thermodynamical stability of vacancies in graphene. The probabilities of three categories of vacancy evolutions (migration, coalescence, and dissociation) are reflected by corresponding reaction rates, which are determined by the energy barriers. Among those evolutions, vacancy migration is the most likely to happen due to its smallest energy barrier, and vacancies can also coalesce sometimes. However, it is extremely difficult for multiple vacancies to dissolve during the whole evolution because of its largest energy barrier. The influences of different factors on vacancy evolution have been investigated, where the energy barrier for vacancy coalescence E_c is found to be dominant. For systems with a low E_c, it is easy for two vacancies to coalesce together when they are neighbors, which makes the ultimate vacancy distribution logarithmic with most of the vacancies being bivacancies, different from the initial distribution where most vacancies are monovacancies. As for the energy barrier for migration and dissociation, both of them hardly affect the vacancy evolutions and so does the initial vacancy proportion. Besides, the temperature also has a slight influence on the ultimate vacancy distribution. These findings reveal the previous elusive evolution of vacancies in graphene, show the stability of vacancy distribution, and are conducive to investigating the evolution mechanism of defects in other 2D materials. In addition, our work provides hints to control vacancy evolution and change vacancy numbers. For example, one may adjust the energy barrier for vacancy coalescence somehow (e.g., by applying additional stress or adding functional groups), and thus, the desired vacancy distribution (unchanged, logarithmic, or others) after the evolution is achievable.

3. METHODS

In the KMC simulations, the graphene is a rhombus with a length of 123.022 nm and a height of 106.54 nm, characterized by the size l_x = 500, which indicates the number of rhombic primitive cells (with a length of 0.246044 nm and a height of 0.213080 nm) along the basis vectors (one in the x-axis). To optimize computing resources and ensure the correctness of simulation results, test simulations with a series of l_x have been performed, whose results are shown in Figure S1. For a high energy barrier for vacancy coalescence E_c, the ultimate vacancy distributions are nearly the same as systems with different sizes. However, for a low E_c, the ultimate vacancy distributions converge with the increase of l_x, and it hardly changes for l_x = 500, which, therefore, is selected as the final graphene size.

The simulations of the evolution of vacancies in monolayer graphene are performed using a homemade KMC program, whose algorithm flowchart is shown in Figure 2. For pristine perfect graphene, every carbon atom is mapped into a lattice site with three nearest-neighbor sites and 6 s-nearest ones and so does every vacancy. For convenience, only the movement of vacancy is considered in the simulations, that is, the migration of one carbon atom to one nearest vacancy site is treated as the migration of this vacancy in the opposite direction. According to the surrounding environment of a vacancy, it may have various possible evolution events as shown in Table 1. For example, if the three nearest sites of a vacancy are all occupied by carbon atoms, there will be three different events for this vacancy because it can migrate to any of the three nearest sites and has different ultimate coordinates..

■ ASSOCIATED CONTENT

Supporting Information

The Supporting Information is available free of charge at https://pubs.acs.org/doi/10.1021/acsomega.2c04121.

Distributions of vacancy type after the vacancy evolution in graphene for different graphene sizes (PDF)

■ AUTHOR INFORMATION

Corresponding Author

Jianming Xue − *State Key Laboratory of Nuclear Physics and Technology, School of Physics and CAPT, HEDPS and IFSA, College of Engineering, Peking University, Beijing 100871, P. R. China*; Email: jmxue@pku.edu.cn

Authors

Shihao Su − *State Key Laboratory of Nuclear Physics and Technology, School of Physics and CAPT, HEDPS and IFSA, College of Engineering, Peking University, Beijing 100871, P. R. China*; orcid.org/0000-0001-7568-2155

Yong Liu − *State Key Laboratory of Nuclear Physics and Technology, School of Physics and CAPT, HEDPS and IFSA, College of Engineering, Peking University, Beijing 100871, P. R. China*

Man Li − *State Key Laboratory of Nuclear Physics and Technology, School of Physics and CAPT, HEDPS and IFSA, College of Engineering, Peking University, Beijing 100871, P. R. China*

Huaqing Huang − *State Key Laboratory of Nuclear Physics and Technology, School of Physics and CAPT, HEDPS and IFSA, College of Engineering, Peking University, Beijing 100871, P. R. China*; orcid.org/0000-0002-7048-4640

Complete contact information is available at: https://pubs.acs.org/10.1021/acsomega.2c04121

https://doi.org/10.1021/acsomega.2c04121
ACS Omega 2022, 7, 36379−36386

Author Contributions

S.S. and Y.L. contributed equally. J.X. conceived the research. S.S. and M.L. performed the theoretical simulations. Y.L. and H.H. wrote the KMC simulation program. All the authors discussed the results and prepared the manuscript.

Notes

The authors declare no competing financial interest.

■ ACKNOWLEDGMENTS

This work is supported by the National Natural Science Foundation of China (grant no. 11775005) and the Science Challenge Project (no. TZ2018004). The authors are grateful for the computing resources provided by the High Performance Computing Platform of the Center for Life Science of Peking University and the Weiming no. 1 and Life Science no. 1 High Performance Computing Platform at Peking University.

■ REFERENCES

(1) Akinwande, D.; Huyghebaert, C.; Wang, C.-H.; Serna, M. I.; Goossens, S.; Li, L.-J.; Wong, H.-S. P.; Koppens, F. H. L. Graphene and two-dimensional materials for silicon technology. *Nature* **2019**, *573*, 507−518.

(2) Tanabe, Y.; Ito, Y.; Sugawara, K.; Koshino, M.; Kimura, S.; Naito, T.; Johnson, I.; Takahashi, T.; Chen, M. Dirac Fermion Kinetics in 3D Curved Graphene. *Adv. Mater.* **2020**, *32*, 2005838.

(3) Yang, Y.; Yang, X.; Liang, L.; Gao, Y.; Cheng, H.; Li, X.; Zou, M.; Ma, R.; Yuan, Q.; Duan, X. Large-Area Graphene-Nanomesh/Carbon-Nanotube Hybrid Membranes for Ionic and Molecular Nanofiltration. *Science* **2019**, *364*, 1057−1062.

(4) Pakulski, D.; Czepa, W.; Buffa, S. D.; Ciesielski, A.; Samorì, P. Atom-Thick Membranes for Water Purification and Blue Energy Harvesting. *Adv. Funct. Mater.* **2020**, *30*, 1902394.

(5) Cheng, C.; Iyengar, S. A.; Karnik, R. Molecular size-dependent subcontinuum solvent permeation and ultrafast nanofiltration across nanoporous graphene membranes. *Nat. Nanotechnol.* **2021**, *16*, 989−995.

(6) Shen, L.; Shi, Q.; Zhang, S.; Gao, J.; Cheng, D. C.; Yi, M.; Song, R.; Wang, L.; Jiang, J.; Karnik, R.; Zhang, S. Highly porous nanofiber-supported monolayer graphene membranes for ultrafast organic solvent nanofiltration. *Sci. Adv.* **2021**, *7*, No. eabg6263.

(7) Shen, J.; Liu, G.; Han, Y.; Jin, W. Artificial Channels for Confined Mass Transport at the Sub-Nanometre Scale. *Nat. Rev. Mater.* **2021**, *6*, 294−312.

(8) Bocquet, L. Nanofluidics Coming of Age. *Nat. Mater.* **2020**, *19*, 254−256.

(9) Tian, X.; Kim, D. S.; Yang, S.; Ciccarino, C. J.; Gong, Y.; Yang, Y.; Yang, Y.; Duschatko, B.; Yuan, Y.; Ajayan, P. M.; Idrobo, J. C.; Narang, P.; Miao, J. Correlating the three-dimensional atomic defects and electronic properties of two-dimensional transition metal dichalcogenides. *Nat. Mater.* **2020**, *19*, 867−873.

(10) Li, W.; Zhan, X.; Song, X.; Si, S.; Chen, R.; Liu, J.; Wang, Z.; He, J.; Xiao, X. A Review of Recent Applications of Ion Beam Techniques on Nanomaterial Surface Modification: Design of Nanostructures and Energy Harvesting. *Small* **2019**, *15*, 1901820.

(11) Mallet, P.; Chiapello, F.; Okuno, H.; Boukari, H.; Jamet, M.; Veuillen, J.-Y. Bound Hole States Associated to Individual Vanadium Atoms Incorporated into Monolayer WSe_2. *Phys. Rev. Lett.* **2020**, *125*, 036802.

(12) Liu, H.; Grasseschi, D.; Dodda, A.; Fujisawa, K.; Olson, D.; Kahn, E.; Zhang, F.; Zhang, T.; Lei, Y.; Branco, R. B. N.; Elías, A. L.; Silva, R. C.; Yeh, Y.-T.; Maroneze, C. M.; Seixas, L.; Hopkins, P.; Das, S.; de Matos, C. J. S.; Terrones, M. Spontaneous chemical functionalization via coordination of Au single atoms on monolayer MoS_2. *Sci. Adv.* **2020**, *6*, No. eabc9308.

(13) Sun, P. Z.; Yagmurcukardes, M.; Zhang, R.; Kuang, W. J.; Lozada-Hidalgo, M.; Liu, B. L.; Cheng, H.-M.; Wang, F. C.; Peeters, F. M.; Grigorieva, I. V.; Geim, A. K. Exponentially selective molecular sieving through angstrom pores. *Nat. Commun.* **2021**, *12*, 7170.

(14) An, Y.; Oliveira, A. F.; Brumme, T.; Kuc, A.; Heine, T. Stone−Wales Defects Cause High Proton Permeability and Isotope Selectivity of Single-Layer Graphene. *Adv. Mater.* **2020**, *32*, 2002442.

(15) Cheng, P.; Kelly, M. M.; Moehring, N. K.; Ko, W.; Li, A.-P.; Idrobo, J. C.; Boutilier, M. S. H.; Kidambi, P. R. Facile Size-Selective Defect Sealing in Large-Area Atomically Thin Graphene Membranes for Sub-Nanometer Scale Separations. *Nano Lett.* **2020**, *20*, 5951−5959.

(16) Epsztein, R.; DuChanois, R. M.; Ritt, C. L.; Noy, A.; Elimelech, M. Towards Single-Species Selectivity of Membranes with Sub-nanometre Pores. *Nat. Nanotechnol.* **2020**, *15*, 426−436.

(17) Xue, L.; Yamazaki, H.; Ren, R.; Wanunu, M.; Ivanov, A. P.; Edel, J. B. Solid-state nanopore sensors. *Nat. Rev. Mater.* **2020**, *5*, 931−951.

(18) Arjmandi-Tash, H.; Belyaeva, L. A.; Schneider, G. F. Single molecule detection with graphene and other two-dimensional materials: nanopores and beyond. *Chem. Soc. Rev.* **2016**, *45*, 476−493.

(19) Banhart, F.; Kotakoski, J.; Krasheninnikov, A. V. Structural Defects in Graphene. *ACS Nano* **2011**, *5*, 26−41.

(20) Li, Z.; Chen, F. Ion beam modification of two-dimensional materials: Characterization, properties, and applications. *Appl. Phys. Rev.* **2017**, *4*, 011103.

(21) Skowron, S. T.; Lebedeva, I. V.; Popov, A. M.; Bichoutskaia, E. Energetics of atomic scale structure changes in graphene. *Chem. Soc. Rev.* **2015**, *44*, 3143−3176.

(22) Su, S.; Wang, X.; Xue, J. Nanopores in Two-Dimensional Materials: Accurate Fabrication. *Mater. Horiz.* **2021**, *8*, 1390−1408.

(23) Vinchon, P.; Glad, X.; Robert Bigras, G.; Martel, R.; Stafford, L. Preferential self-healing at grain boundaries in plasma-treated graphene. *Nat. Mater.* **2021**, *20*, 49−54.

(24) Girit, Ç. Ö.; Meyer, J. C.; Erni, R.; Rossell, M. D.; Kisielowski, C.; Yang, L.; Park, C.-H.; Crommie, M. F.; Cohen, M. L.; Louie, S. G.; Zettl, A. Graphene at the Edge: Stability and Dynamics. *Science* **2009**, *323*, 1705−1708.

(25) Zan, R.; Ramasse, Q. M.; Bangert, U.; Novoselov, K. S. Graphene Reknits Its Holes. *Nano Lett.* **2012**, *12*, 3936−3940.

(26) Voter, A. F.*Radiation Effects in Solids*; Springer, 2007; pp 1−23.

(27) Zhang, L.; Han, J.; Wang, H.; Car, R.; E, W. Deep Potential Molecular Dynamics: A Scalable Model with the Accuracy of Quantum Mechanics. *Phys. Rev. Lett.* **2018**, *120*, 143001.

(28) Henkelman, G.; Jónsson, H. Improved tangent estimate in the nudged elastic band method for finding minimum energy paths and saddle points. *J. Chem. Phys.* **2000**, *113*, 9978−9985.

(29) Becquart, C.; Domain, C. An object Kinetic Monte Carlo Simulation of the dynamics of helium and point defects in tungsten. *J. Nucl. Mater.* **2009**, *385*, 223−227.

(30) Guo, X.; Zhang, X.; Xue, J.; Li, W. KMC simulation of helium bubble formation in alpha-Fe. *Nucl. Instrum. Methods Phys. Res., Sect. B* **2013**, *307*, 77−80.

(31) Momeni, K.; Ji, Y.; Wang, Y.; Paul, S.; Neshani, S.; Yilmaz, D. E.; Shin, Y. K.; Zhang, D.; Jiang, J.-W.; Park, H. S.; Sinnott, S.; van Duin, A.; Crespi, V.; Chen, L.-Q. Multiscale computational understanding and growth of 2D materials: a review. *npj Comput. Mater.* **2020**, *6*, 22.

(32) Chen, S.; Gao, J.; Srinivasan, B. M.; Zhang, G.; Sorkin, V.; Hariharaputran, R.; Zhang, Y.-W. A kinetic Monte Carlo model for the growth and etching of graphene during chemical vapor deposition. *Carbon* **2019**, *146*, 399−405.

(33) Kong, X.; Zhuang, J.; Zhu, L.; Ding, F. The complementary graphene growth and etching revealed by large-scale kinetic Monte Carlo simulation. *npj Comput. Mater.* **2021**, *7*, 14.

(34) Muralidharan, P.; Goodnick, S. M.; Vasileska, D. Kinetic Monte Carlo simulation of transport in amorphous silicon passivation layers in silicon heterojunction solar cells. *J. Comput. Electron.* **2019**, *18*, 1152−1161.

https://doi.org/10.1021/acsomega.2c04121
ACS Omega 2022, 7, 36379−36386

(35) Trevethan, T.; Latham, C. D.; Heggie, M. I.; Briddon, P. R.; Rayson, M. J. Vacancy diffusion and coalescence in graphene directed by defect strain fields. *Nanoscale* **2014**, *6*, 2978−2986.
(36) Parisi, L.; Di Giugno, R.; Deretzis, I.; Angilella, G.; La Magna, A. Kinetic Monte Carlo simulations of vacancy evolution in graphene. *Mater. Sci. Semicond. Process.* **2016**, *42*, 179−182.
(37) Govind Rajan, A.; Silmore, K. S.; Swett, J.; Robertson, A. W.; Warner, J. H.; Blankschtein, D.; Strano, M. S. Addressing the Isomer Cataloguing Problem for Nanopores in Two-Dimensional Materials. *Nat. Mater.* **2019**, *18*, 129−135.
(38) Vineyard, G. H. Frequency factors and isotope effects in solid state rate processes. *J. Phys. Chem. Solids* **1957**, *3*, 121−127.
(39) Battaile, C. C. The Kinetic Monte Carlo method: Foundation, implementation, and application. *Comput. Methods Appl. Mech. Eng.* **2008**, *197*, 3386−3398.
(40) Andersen, M.; Panosetti, C.; Reuter, K. A practical guide to surface kinetic Monte Carlo simulations. *Front. Chem.* **2019**, *7*, 202.
(41) He, K.; Robertson, A. W.; Gong, C.; Allen, C. S.; Xu, Q.; Zandbergen, H.; Grossman, J. C.; Kirkland, A. I.; Warner, J. H. Controlled formation of closed-edge nanopores in graphene. *Nanoscale* **2015**, *7*, 11602−11610.
(42) Robertson, A. W.; Lee, G.-D.; He, K.; Gong, C.; Chen, Q.; Yoon, E.; Kirkland, A. I.; Warner, J. H. Atomic Structure of Graphene Subnanometer Pores. *ACS Nano* **2015**, *9*, 11599−11607.
(43) Su, S.; Xue, J. Facile Fabrication of Subnanopores in Graphene under Ion Irradiation: Molecular Dynamics Simulations. *ACS Appl. Mater. Interfaces* **2021**, *13*, 12366−12374.
(44) Su, S.; Zhang, Y.; Peng, S.; Guo, L.; Liu, Y.; Fu, E.; Yao, H.; Du, J.; Du, G.; Xue, J. Multifunctional Graphene Heterogeneous Nanochannel with Voltage-Tunable Ion Selectivity. *Nat. Commun.* **2022**, *13*, 4894.

https://doi.org/10.1021/acsomega.2c04121
ACS Omega 2022, 7, 36379−36386